Effects of disorder on the intrinsically hole-doped iron-based superconductor $KCa_2Fe_4As_4F_2$ by cobalt substitution

Junichi Ishida,[1] Soshi Iimura,[1,*] and Hideo Hosono[1,2,†]

[1]*Laboratory for Materials and Structures, Tokyo Institute of Technology, 4259 Nagatsuta-cho, Midori-ku, Yokohama 226-8503, Japan*

[2]*Materials Research Center for Element Strategy, Tokyo Institute of Technology, 4259 Nagatsuta-cho, Midori-ku, Yokohama 226-8503, Japan*

(Received 29 September 2017; published 27 November 2017)

In this paper, the effects of cobalt substitution on the transport and electronic properties of the recently discovered iron-based superconductor $KCa_2Fe_4As_4F_2$, with $T_c = 33$ K, are reported. This material is an unusual superconductor showing intrinsic hole conduction (0.25 holes/Fe^{2+}). Upon doping of Co, the T_c of $KCa_2(Fe_{1-x}Co_x)_4As_4F_2$ gradually decreased, and bulk superconductivity disappeared when $x \geqslant 0.25$. Conversion of the primary carrier from *p* type to *n* type upon Co-doping was clearly confirmed by Hall measurements, and our results are consistent with the change in the calculated Fermi surface. Nevertheless, neither spin density wave (SDW) nor an orthorhombic phase, which are commonly observed for nondoped iron-based superconductors, was observed in the nondoped or electron-doped samples. The electron count in the 3*d* orbitals and structural parameters were compared with those of other iron-based superconductors to show that the physical properties can be primarily ascribed to the effects of disorder.

DOI: 10.1103/PhysRevB.96.174522

I. INTRODUCTION

Doping is an effective method for developing the physical properties of Fe-based superconductors (FeSCs) [1,2]. Electronic states show a strong dependence on carrier density and structural parameters; hence, various types of alio- and isovalent doping approaches have been applied to the Fe and other sites of FeSCs. Carrier doping into the parent compound breaks the spin density wave (SDW)-driven antiferromagnetic phase and induces superconductivity [3–5]. Unlike the case of overdoped cuprates, a considerable increase of the electronic correlation is observed in heavily electron-doped $SmFeAsO_{1-x}H_x$ and heavily hole-doped $Ba_{1-x}K_xFe_2As_2$, which suggests the potential for unique physics in FeSC [6,7]. However, the substitution of isovalent atoms displaces atoms in the crystal structure without changing the carrier density, which can also lead to superconductivity. Phase diagrams analogous to carrier-doped FeSCs have been reported in $Ba(Fe_{1-x}Ru_x)_2As_2$ and $BaFe_2(As_{1-x}P_x)_2$ [8–11]. Another important factor tuning the electronic properties is local disorder, which derives from the effects of substituted atoms and lattice defects. The introduction of disorder usually affects both the superconducting and the magnetic transition temperatures [12–15]. Because the interactions between Cooper pairs and impurities strongly depend on the symmetry of the superconducting gap function, the effects of disorder on T_c are material dependent and vary among FeSCs.

Although a variety of physical properties can be tuned through physical parameters, it is quite difficult to obtain a general understanding of individual effects owing to the complex interdependencies of charge, crystal structure, and disorder. In particular, the effects of disorder remain controversial. When disorder is introduced by impurity doping, it changes the carrier density and lattice parameters; hence, isolating the effects of disorder is difficult. One strategy to overcome this obstacle is to compare the physical properties with those of other FeSCs, which have the same carrier density and lattice parameters. From this perspective, papers on the charge compensated $Ba_{1-x}K_x(Fe_{1-x/2}Co_{x/2})_2As_2$ have provided intriguing results [16,17]. Although the same amounts of holes and electrons are doped into the parent $BaFe_2As_2$ compound, SDW order does not develop and superconductivity emerges instead. This result provides evidence for the validity of theories that predict suppression of SDW and emergence of superconductivity can be induced by only the introduction of disorder without the change of carrier concentration [18,19]. Although the role of disorder on 122 systems has been clearly shown by impurity substitution or electron irradiation methods [13–15], it is important to examine how disorder affects the electronic states of other systems with different compositions and crystal structures. In this paper, we focus on the new class of FeSCs that has been recently reported [20]. The inset of Fig. 1(a) shows the crystal structure of the 12442-type compound, $KCa_2Fe_4As_4F_2$. It has a superstructure composed of 1111-type CaFeAsF and 122-type KFe_2As_2, which is an end member of the hole-doped $Ba_{1-x}K_xFe_2As_2$ system [21,22]. Consequently, the formal charge of Fe in the 12442 type is given as +2.25, which means that the 12442 type belongs to a rare class of intrinsically hole-doped FeSCs (0.25 holes/Fe^{2+}). Tuning the carrier type from holes to electrons by impurity substitution, we evaluated the effects of disorder, comparing the electron count in the 3*d* orbitals and structural parameters with other systems. Whereas changes of T_c (30–37 K) have been reported for isomorphs such as $ALnFe_4As_4O_2$ and $ACaFe_4As_4F_2$ (A = alkali metal; Ln = lanthanides) [20,23–25], no phase diagram for the 12442 system has been reported to date.

In this paper, we selected $KCa_2Fe_4As_4F_2$ and substituted Co into Fe sites to investigate the variation of transport and electronic properties with electron doping (hereafter, $KCa_2(Fe_{1-x}Co_x)_4As_4F_2$ is abbreviated as 12442). Chemical composition analysis, x-ray diffraction (XRD), and measurements of resistivity, magnetic susceptibility, the Hall effect, and specific heat were performed, together with density

*Corresponding author: s_iimura@mces.titech.ac.jp

†Corresponding author: hosono@msl.titech.ac.jp

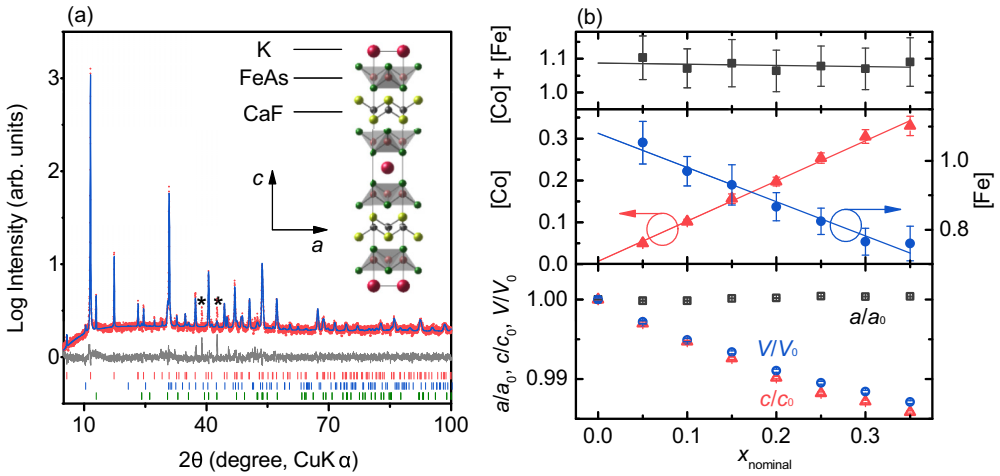

FIG. 1. (a) Rietveld refinement with powder XRD of the $KCa_2(Fe_{1-x}Co_x)_4As_4F_2$ ($x_{nominal} = 0.3$) polycrystalline sample at room temperature. Peak positions of the main phase and impurities KFe_2As_2 and CaFeAsF are represented by red, blue, and green bars, respectively. Asterisks denote the peak positions of undetermined impurities. Inset shows the crystal structure of $KCa_2Fe_4As_4F_2$. (b) Atomic concentrations determined from EPMA measurements, normalized lattice parameters, and the cell volume for the nominal Co-doping [$a_0 = 3.86882(16)$ Å, $c_0 = 31.00516(19)$ Å, $V_0 = 486.862(74)$ Å^3]. The EPMA results and compositional analysis demonstrated contamination by oxygen; thus, the real chemical formula becomes $KCa_2(Fe_{1-x}Co_x)_4As_4F_2O_y$($y \approx 0.5$). Because the oxygen contents were almost same for all samples, we ascribed the systematic change of the physical properties to the Co substitution effects and neglected contamination effects.

functional theory (DFT) calculations. Co-doping suppressed the T_c of the system, and the bulk superconductivity disappeared at $x = 0.25(1)$ doping. The carrier type was converted from hole to electron, indicating that Co behaves as an electron dopant. No structural and/or magnetic transitions were observed in the x range from 0 to 0.33(2), although the electron count of the Fe-3d orbitals and the topology of the Fermi surface (FS) showed similarities to those of nondoped LaFeAsO and $BaFe_2As_2$ as x approached ~0.1. Through a comparison of the phase diagram of $Ba_{1-x}K_x(Fe_{1-y}Co_y)_2As_2$ with the T_c change of $KCa_2(Fe_{1-x}Co_x)_4As_4F_2$, we show that the underlying physics of these materials are the same and their characteristic physical properties above can be ascribed to disorder.

II. EXPERIMENTAL DETAILS

Polycrystalline $KCa_2(Fe_{1-x}Co_x)_4As_4F_2$ was synthesized by solid-state reaction methods with the use of KAs, CaAs, CaF_2, Fe_2As, and Co_2As. Mixtures of these ingredients were grained and pelletized in an Ar filled (H_2O, O_2 <1 ppm) glove box (Miwa Manufacturing). The mixtures were placed in boron nitride tubes and sealed in Ar filled stainless steel sample containers. The samples were heated to 1203 K for 9.5 h, soaked at that temperature for 30 h, and then quenched. Crystalline phases were identified by powder XRD with CuKα radiation (Bruker AXS, D8 Advance-TXS with a Cu rotating anode). Rietveld analysis of the XRD patterns was performed using the TOPAS code. The chemical compositions were determined with an electron probe microanalyzer (EPMA, JXA-8530F, JEOL) equipped with a field emission electron gun and wavelength dispersive x-ray detectors. The longitudinal (ρ_{xx}) and transverse (ρ_{xy}) resistivity data were measured with a Physical Property Measurement System (PPMS; Quantum Design) by the four-probe technique. The magnetic susceptibility was measured with a vibrating sample magnetometer attachment (Magnetic Property Measurement System [MPMS]; Quantum Design). The specific heat (C_p) was measured in the PPMS by a relaxation technique. The electronic structure for $KCa_2(Fe_{1-x}Co_x)_4As_4F_2$ was evaluated by non-spin-polarized DFT calculations with the use of the full-potential linearized, augmented plane wave plus the localized orbitals method implemented in WIEN2k code. For the generalized gradient approximation, the Perdew-Burke-Ernzerhof functional was adopted. To ensure convergence, the linearized, augmented plane wave basis set was defined by the cutoff $RMTKMAX = 9.0$ (RMT: the smallest atomic sphere radius in the unit cell), with a mesh sampling of 21 × 21 × 21 k points in the Brillouin zone. The electron doping via the partial cobalt substitution for the Fe site was modeled by the virtual crystal approximation (VCA), which assumes that Fe ($Z = 26$) behaves as a virtual atom with a fractional nuclear charge ($Z = 26 + x$).

In addition to Co substitution, we examined various doping modes, including Ba, Na, La, and H doping for K, Ca, Ca, and F sites, respectively. For H substitution, a high-pressure synthesis technique was used at 5 GPa. However, none of these substitutions were successful. Although syntheses of $RbGd_2Fe_4As_4O_2$ and its H-substituted samples were also attempted with the high-pressure technique, the 12442 phase was not obtained at 2 or 5 GPa.

III. RESULTS AND DISCUSSION

A. Chemical composition and structural analyses

Figure 1(a) shows the XRD patterns and results of Rietveld fitting of the Co-substituted $KCa_2(Fe_{1-x}Co_x)_4As_4F_2$ with a nominal x($x_{nominal}$) value of 0.3. The crystal structures for all x compositions were refined with the tetragonal space group $I4/mmm$. The impurity phases were CaFeAsF and KFe_2As_2, and an undetermined phase was observed above $x_{nominal}$ =

0.20. Over $x_{\text{nominal}} = 0.35$, the 12442 phase vanished; hence, we concluded that the solubility limit of Co for the Fe site was located around $x_{\text{nominal}} = 0.35$. The peak intensities for the undetermined peaks did not show any relationship with the doping level, indicating that those peaks were related not to a structural change of the 12442 phase but rather to undetermined impurities. We confirmed by the detailed XRD measurement that Co atoms were homogeneously substituted for each FeAs layer of 1111 and 122 sublattices. If the substitution was performed inequivalently for the FeAs layer of the 1111-type or 122-type part, the space group of the crystal structure would be reduced from $I4/mmm$ to $P4/mmm$; however, we found no additional peaks derived from the $P4/mmm$ structure, as shown in Fig. S1 in the Supplemental Material [26]. Successful Co-doping of the 12442 phase was confirmed by the EPMA measurements [Fig. 1(b)]. Upon doping, the corresponding measured Co content, [Co] increased linearly while [Fe] decreased. The sum of these contents, [Co] + [Fe], took a value of approximately 1, indicating that Co substituted Fe sites. Hereafter, we use the analyzed cobalt content [Co] as x. The x_{nominal} dependence of the normalized lattice constants a/a_0 and c/c_0 and the cell volume V/V_0 measured relative to the values of nondoped samples are summarized at the bottom of Fig. 1(b). The value of a/a_0 remained almost constant as x_{nominal} changed, while c/c_0 showed a monotonic decrease. This trend is a common feature of Co-doped Fe-pnictide superconductors because of the smaller ionic radii of Co^{2+} compared with that of Fe^{2+} [21,27,28]. Figure S2 in the Supplemental Material [26] summarizes the bond lengths ($d_{\text{Fe-As}}$), bond angles ($\alpha_{\text{As-Fe-As}}$), and arsenic heights (h_{As}) around the two arsenic sites, As(1) and As(2), as a function of x. The parameters $\alpha_{\text{As1(2)-Fe-As1(2)}}$ and $h_{\text{As1(2)}}$ varied with Co-doping over a narrow range of 107.7°–111.0° (108.2°–111.3°) and 1.33–1.40 Å (1.32–1.39 Å), respectively. The x variation of the parameters $\alpha_{\text{As1(2)-Fe-As1(2)}}$ and $h_{\text{As1(2)}}$ was close to 109.47° and 1.38 Å, respectively, which are the optimal values giving the highest-T_c superconductivity in Fe pnictides (see Supplemental Material [26]). These results indicate that the crystal structures of the 12442 samples were close to the optimal parameters for superconductivity.

B. Transport and magnetic properties

Figure 2 shows the results of the electrical resistivity and magnetic susceptibility measurements. Upon Co-doping, T_c was monotonically suppressed and disappeared in the overdoped region. Each T_c value obtained by conductivity and susceptibility measurements is summarized in the top panel of Fig. 2(c). Although a superconducting transition was clearly observed for the $x = 0.25(1)$ sample in the resistivity measurements, the magnetic shielding effect persisted up to $x = 0.20(1)$, above which there was no Meissner signal [Figs. 2(a) and 2(b)]. For superconducting samples, the volume fraction was approximately 100% in the underdoped region and decreased to ~80% and ~40% for sample compositions $x = 0.15(1)$ and $0.20(1)$, respectively [Fig. 2(b) and Fig. S3 in the Supplemental Material [26]]. This result indicates that bulk superconductivity exists in the composition range $x = 0.00 - -0.20(1)$, while filamentary superconductivity occurs for $x \geqslant 0.25(1)$. The temperature dependence of the

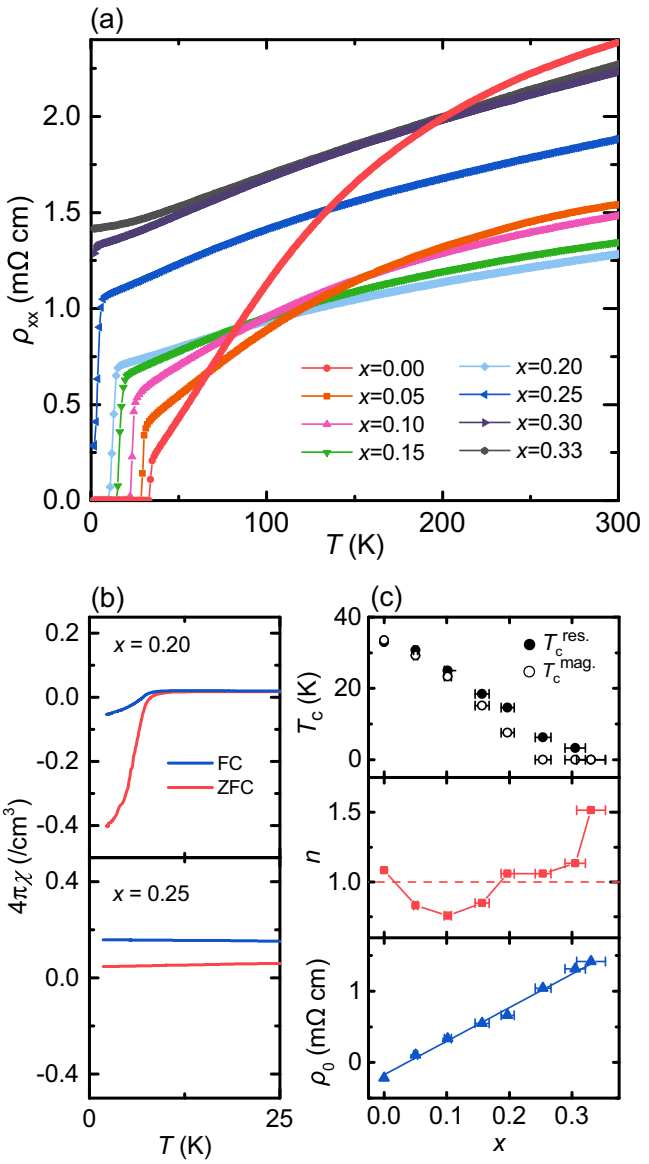

FIG. 2. (a) Temperature dependence of the resistivity ρ_{xx} for each x composition. (b) Temperature dependence of the magnetic susceptibility in a field of 10 Oe for $x = 0.20(0)$ (top) and $x = 0.25(1)$ (bottom) samples. Blue and red lines represent the field-cooled and zero-field-cooled conditions, respectively. (c) Doping dependence of the two types of T_c, T_c^{res} (closed circles) and T_c^{mag} (open circles), obtained from the electronic resistivity and magnetic susceptibility measurements, respectively (top panel); the exponent n of the fitting function $\rho_{xx} = \rho_0 + AT^n$ with a red dashed guideline at $n = 1$ (middle panel); and the residual resistivity ρ_0 (bottom panel).

normal state resistivity was also modulated by Co-doping. In the pristine sample, ρ_{xx} showed concave behavior similar to hole-doped high-T_c FeSCs such as $Ba_{1-x}K_xFe_2As_2$ [4]. Upon doping, the temperature dependence became less pronounced and the concave feature transformed into a convex shape, particularly in the low temperature region. As shown in Fig. 2(a), there was no sudden change of ρ_{xx} above T_c, and the derivative of ρ_{xx} showed no sign of a phase transition (Fig. S4 in the Supplemental Material). These results indicate the absence of magnetostructural transition characteristics in the parent phase

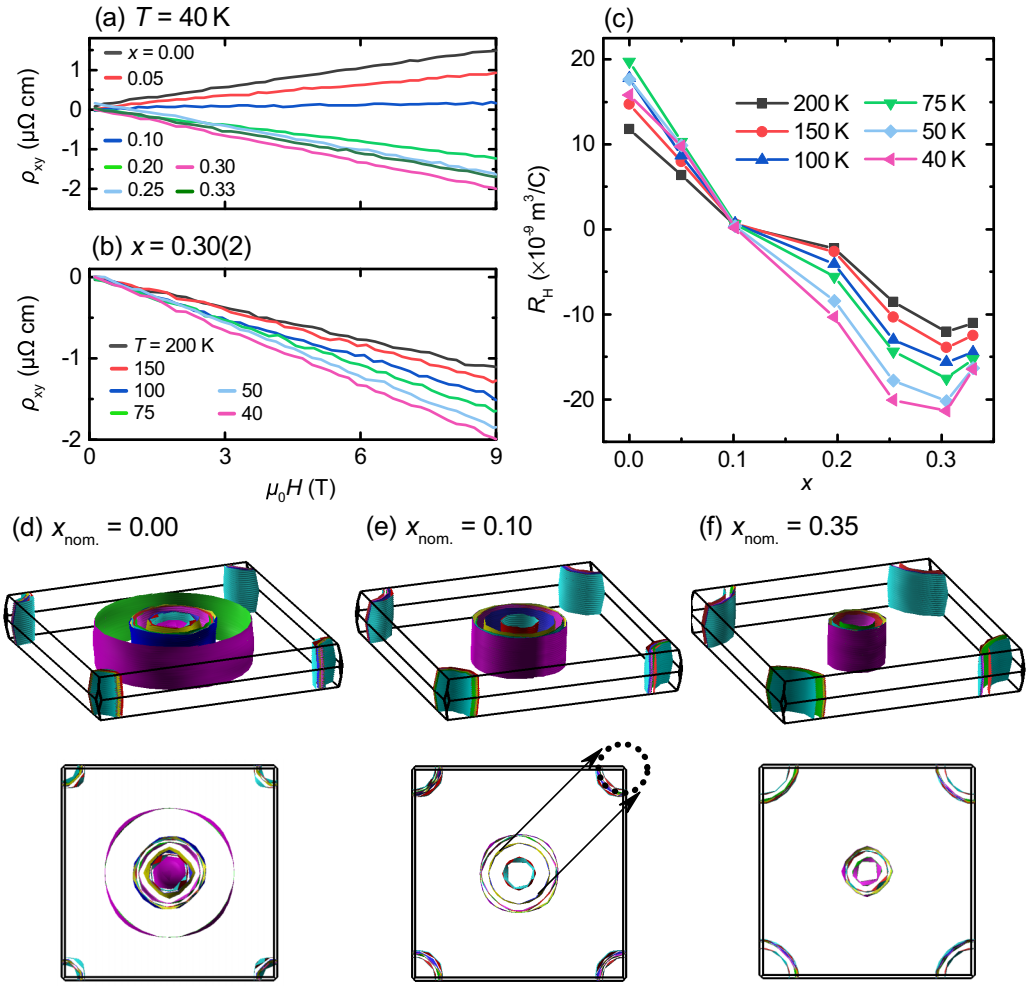

FIG. 3. Field dependence of the hole resistivity for $KCa_2(Fe_{1-x}Co_x)As_4F_2$ at (a) $T = 40$ K and for (b) $x = 0.30(2)$. (c) Co-doping dependence of the Hall coefficient R_H for various temperatures. (d)–(f) Calculated FSs for $x_{nominal} = 0.00$, 0.10, and 0.35, respectively, using the VCA. Top views are also shown below the FSs. Black solid arrows in (e) represent possible nesting vectors between the hole and the electron surfaces.

of the FeSCs. To evaluate the resistivity curves in detail, we analyzed the data using the fitting function $\rho_{xx} = \rho_0 + AT^n$ at low temperatures, where ρ_0 is the residual resistivity. As shown in the middle panel of Fig. 2(c), the exponent n takes a value of approximately 1 in the pristine sample, which is characteristic of a non-Fermi liquid. In the doped region above $x = 0.10(0)$, the value of n gradually increased, indicating that the system approached a conventional Fermi liquid. However, ρ_0 linearly increased with x, demonstrating that the substituted Co behaved as an impurity scattering center in this system.

Figure 3 shows the Hall resistivity ρ_{xy}, Hall coefficient R_H, and calculated FS for various compositions and temperatures. As reported by Wang *et al.* [20], the nondoped sample showed hole conductivity, as evident from the positive slope in the field dependence of ρ_{xy} for $x = 0.00$ [Figs. 3(a) and 3(b)]. With increasing Co content, the sign changed from positive to negative around $x = 0.10(0)$. This result clearly indicates that the doped Co behaved as an electron dopant and converted the carrier type from holes to electrons. The FeSCs have a semimetallic band structure consisting of hole and electron FSs; hence, ρ_{xy} is expressed by following two-band model [29]:

$$\rho_{xy}(H) = \frac{\sigma_h^2 R_{Hh} + \sigma_e^2 R_{He} + \sigma_h^2\sigma_e^2 R_{Hh}R_{He}(R_{Hh}+R_{He})H^2}{(\sigma_h+\sigma_e)^2 + \sigma_h^2\sigma_e^2(R_{Hh}+R_{He})^2H^2} H. \quad (1)$$

Here, σ_i, R_{Hi} ($i = h$ or e) and H are the conductivity, Hall coefficient for each carrier, and magnetic field, respectively. The linear response seen in Figs. 3(a) and 3(b) suggests that the nonlinearity term, $R_{Hh} + R_{He}$, is negligible. This assumption directly indicates that the 12442 samples for each Co content are in the proximity of a compensated semimetal; i.e., the electron and hole concentrations are balanced. In this case, the Hall coefficient can be reduced to

$$R_H = \frac{1}{e}\frac{N_e\mu_e^2 - N_h\mu_h^2}{(N\mu_e + N\mu_h)^2}, \quad (2)$$

where N_i and μ_i ($i = h$ or e) are the number of carriers and their mobility, respectively. The values of R_H are close to zero at $x = 0.10(0)$, indicating that complete hole-electron compensation is realized, and their mobilities are equaled

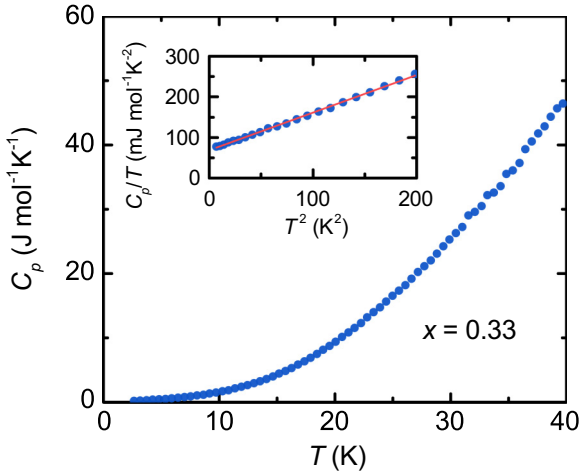

FIG. 4. Low temperature specific heat C_p for the $x = 0.33(2)$ sample. Inset shows the T^2 dependence of C_p/T. Solid red line shows an approximate line.

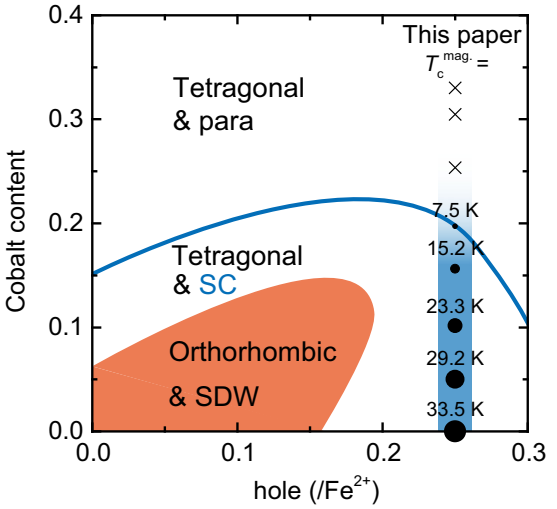

FIG. 5. Phase diagram of the electron- and hole-doped $Ba_{1-x}K_x(Fe_{1-y}Co_y)_2As_2$ with respect to hole and cobalt content [16,17]. Bulk T_c data (represented by T_c^{mag}) of 12442 with cobalt contents were plotted at a corresponding hole-doping level of 0.25 with a light blue guideline. Orange region indicates a parent phase with orthorhombic crystal structure and SDW order in $Ba_{1-x}K_x(Fe_{1-y}Co_y)_2As_2$. The border between the bulk superconducting phase and the paramagnetic metal phase is represented by the blue solid line.

at this composition [Fig. 3(c)]. These results are consistent with the topology of the FS for $x_{nominal} = 0$, 0.10, and 0.35 [Figs. 3(d)–3(f)]. Under the nondoped conditions, large hole pockets exist at the center of the Brillouin zone, with small electron pockets at the corners. Upon electron doping, the radii of each pocket are balanced, and the electron pockets become larger than the hole pockets, corresponding to the sequential positive to negative change of R_H. The SDW transition might be expected to occur when $x \approx 0.1$ because of the good nesting conditions; however, no anomalies indicative of an SDW were observed in our transport experiments. This situation is similar to the case of $LiFe_{1-x}Co_xAs$, in which the nesting conditions are enhanced by Co-doping, while no magnetic transition is observed [30,31]. A detailed discussion of this point is given in a later section.

C. Specific heat measurements

To estimate the degree of electron correlation, we performed specific heat measurements for the overdoped sample with $x = 0.33(2)$. Figure 4 shows the temperature dependence of the C_p at $x = 0.33(2)$ for which no superconductivity was observed above 2 K. As shown in the inset, the C_p/T featured a linear-T^2 dependence; thus, the line could be fitted by the function $C_p/T = \gamma + \beta T^2$, where γ denotes the Sommerfeld coefficient. The obtained value of γ was 68.6(8)mJ mol^{-1}K^{-2} [or 17.2(4)mJ TM-mol^{-1} K^{-2}, where TM represents the transition metal atom that contributes to the electronic C_p]. Table I compares the γ values with those of KFe_2As_2 and Co-overdoped (nonsuperconducting) 111, 122, and 1111 systems [26,32–34] with different electron filling of Fe − 3d orbitals and carrier types. Because the electronic state of the hole-overdoped KFe_2As_2 is in the proximity of the Mott insulating Mn-3d [5] state, the electronic correlation is enhanced, which leads to the largest γ value [7]. Notably, γ for the 12442 system takes a value two or three times larger than those of the Co-doped 111, 122, and 1111 systems, despite having a comparable net electron count to that of other Co-doped systems. This result indicates that γ and electronic correlation are affected by both the electron count and the content of impurity scattering centers (i.e., Co atoms) or that the Co atoms do not donate one electron per Co.

D. Comparison with other FeSC systems

To understand the electronic state in the 12442 system, it is informative to compare its physical properties with those of $Ba_{1-x}K_x(Fe_{1-y}Co_y)_2As_2$, because the electronic state with $x = 0.50$ (0.25 holes/Fe^{2+}) is thought to be similar to our system, and the x-y phase diagram has already been reported, enabling a simple comparison [16,17]. Figure 5 depicts a

TABLE I. Physical and chemical properties of KFe_2As_2, $KCa_2(Fe_{0.67}Co_{0.33})_4As_4F_2$, $NaFe_{0.92}Co_{0.08}As$, $Ba(Fe_{0.86}Co_{0.14})_2As_2$, and $LaFe_{0.80}Co_{0.20}AsO$ systems. N is the electron count of the 3d orbital. Carrier type and Sommerfeld coefficients γ are also given.

	KFe_2As_2	$KCa_2(Fe_{1-x}Co_x)_4As_4F_2$ ($x = 0.33$)	$NaFe_{1-x}Co_xAs$ ($x = 0.08$)	$Ba(Fe_{1-x}Co_x)_2Asx_2$ ($x = 0.14$)	$LaFe_{1-x}Co_xAsO$ ($x = 0.20$)
N	5.5	6.08	6.08	6.14	6.20
Carrier type	Hole	Electron	Electron	Electron	Electron
γ(mJ/TM-mol K^2)	57	17.2	2.75	7.95	5.87

schematic phase diagram of $Ba_{1-x}K_x(Fe_{1-y}Co_y)_2As_2$, where the T_c variation of bulk superconductivity in the 12442 system is plotted at the corresponding hole level as $0.25/Fe^{2+}$. From this line, the Co-doping of both systems do not show any parent phases, such as low temperature orthorhombic and SDW-driven antiferromagnetic phases. These results indicate that these two systems share the same underlying physics.

Here, we discuss two factors that likely cause this phenomenon. First is the structural change associated with the Co-doping. As mentioned above, the optimal parameters are $\alpha_{\text{As-Fe-As}}(109.47^\circ)$ and $h_{\text{As}}(1.38\ \text{Å})$, which give rise to the high T_c, and are located inside the range of variation of those parameters in the 12442 system. Upon Co-doping, the bulk T_c decreases, and superconductivity disappears at $x = 0.25(1)$, where $\alpha_{\text{As1(2)-Fe-As1(2)}}$ and $h_{\text{As1(2)}}$ are given as 109.6° (110.1°) and 1.36 Å (1.35 Å), respectively. This result indicates that although the structural parameters are close to their optimal values, the superconductivity is completely suppressed. Therefore, we suggest that the T_c reduction is not triggered by a change of the structural parameters. Moreover, the effects of the crystal structure alone do not clearly explain the reason for the absence of magnetic transitions despite the good nesting conditions. Thus, it is unlikely that structural changes are the origin of the observed phenomena in the 12442 system.

The second factor is disorder, which derives from substituted Co atoms. Fernandes *et al.* theoretically suggested that the introduction of disorder has contrasting effects in $s^{\pm}$ superconductors (i.e., s-wave superconductors where sign reversal of the gap function occurs): one is the pair-breaking effect, which suppresses superconductivity, and the other is the suppression of the SDW order, which leads to superconductivity [19]. To confirm the applicability of this theory to the 12442 system, we consider the superconducting symmetry of our system. Although detailed measurements of the physical properties of this system have yet to be obtained, the analogous self-doped FeSC, $CaKFe_4As_4$ ($0.25\ \text{holes}/Fe^{2+}$) [35], shows a nodeless $s^{\pm}$-wave state, as indicated by recent London penetration depth, nuclear magnetic resonance (NMR), and angle-resolved photoemission spectroscopy (ARPES) measurements [36–38]. Moreover, $Ba_{0.6}K_{0.4}Fe_2As_2$, in which holes are doped by nearly the same amount ($0.20\ \text{holes}/Fe^{2+}$), is believed to be an $s^{\pm}$ superconductor [39,40]. On the basis of this information, it is reasonable to assume that the superconducting symmetry of the 12442 system has nodeless $s^{\pm}$ − wave symmetry. Therefore, we conclude that the pair-breaking effect by Co-doping overcomes the development of superconductivity derived from the suppressed, fluctuating SDW, leading to the characteristic physical properties in Co-doped 122 and 12442 systems.

IV. SUMMARY

We studied the effects of cobalt substitution on the intrinsically hole-doped FeSC $KCa_2(Fe_{1-x}Co_x)_4As_4F_2$. We revealed that the Co dopant acts not only as an electron dopant but also as an impurity scattering center. The bulk superconductivity was gradually suppressed as x was increased and vanished at $x = 0.25(1)$. The effectiveness of electron doping by Co substitution and the formation of good nesting conditions were confirmed from Hall effect measurements and DFT calculations; however, there was no sign of a magnetostructural phase transition from the measurement of the transport properties. We plotted the T_c variation of the 12442 system on the phase diagram of $Ba_{1-x}K_x(Fe_{1-y}Co_y)_2As_2$, which is thought to have an electronic structure similar to that of our system. The properties of our materials were discussed in terms of electron count, structural parameters, and disorder. The origin of the T_c reduction and the absence of a magnetostructural transition were attributed to the effects of disorder induced by substituted Co atoms. This paper sheds light on the prominent role of disorder in both 12442 and 122 systems and indicates that all doped FeSCs are strongly affected by disorder; however, the effect is usually obscured by the effects of charge and structural parameters.

ACKNOWLEDGMENTS

This paper was supported by the Ministry of Education, Culture, Sports, Science and Technology (MEXT) Elements Strategy Initiative to Form Core Research Center. We thank Andrew Jackson, Ph.D., from the Edanz Group (www.edanzediting.com/ac) for editing a draft of this manuscript.

[1] J. Paglione and R. L. Greene, Nat. Phys. **6**, 645 (2010).
[2] D. C. Johnston, Adv. Phys. **59**, 803 (2010).
[3] Y. Kamihara, T. Watanabe, M. Hirano, and H. Hosono, J. Am. Chem. Soc. **130**, 3296 (2008).
[4] M. Rotter, M. Tegel, and D. Johrendt, Phys. Rev. Lett. **101**, 107006 (2008).
[5] T. Katase, S. Iimura, H. Hiramatsu, T. Kamiya, and H. Hosono, Phys. Rev. B **85**, 140516 (2012).
[6] S. Iimura, H. Okanishi, S. Matsuishi, H. Hiraka, T. Honda, K. Ikeda, T. C. Hansen, T. Otomo, and H. Hosono, Proc. Natl. Acad. Sci. **114**, E4354 (2017).
[7] L. de' Medici, G. Giovannetti, and M. Capone, Phys. Rev. Lett. **112**, 177001 (2014).
[8] A. Thaler, N. Ni, A. Kracher, J. Q. Yan, S. L. Bud'ko, and P. C. Canfield, Phys. Rev. B **82**, 014534 (2010).
[9] S. Sharma, A. Bharathi, S. Chandra, V. R. Reddy, S. Paulraj, A. T. Satya, V. S. Sastry, A. Gupta, and C. S. Sundar, Phys. Rev. B **81**, 174512 (2010).
[10] S. Jiang, H. Xing, G. Xuan, C. Wang, Z. Ren, C. Feng, J. Dai, Z. Xu, and G. Cao, J. Phys. Condens. Matter **21**, 382203 (2009).
[11] S. Kasahara, T. Shibauchi, K. Hashimoto, K. Ikada, S. Tonegawa, R. Okazaki, H. Shishido, H. Ikeda, H. Takeya, K. Hirata, T. Terashima, and Y. Matsuda, Phys. Rev. B **81**, 184519 (2010).
[12] Y. F. Guo, Y. G. Shi, S. Yu, A. A. Belik, Y. Matsushita, M. Tanaka, Y. Katsuya, K. Kobayashi, I. Nowik, I. Felner, V. P. S. Awana, K. Yamaura, and E. Takayama-Muromachi, Phys. Rev. B **82**, 054506 (2010).
[13] R. Prozorov, M. Kończykowski, M. A. Tanatar, A. Thaler, S. L. Bud'ko, P. C. Canfield, V. Mishra, and P. J. Hirschfeld, Phys. Rev. X **4**, 041032 (2014).

[14] K. Cho, M. Kończykowski, S. Teknowijoyo, M. A. Tanatar, Y. Liu, T. A. Lograsso, W. E. Straszheim, V. Mishra, S. Maiti, P. J. Hirschfeld, and R. Prozorov, Sci. Adv. **2**, e1600807 (2016).

[15] Y. Mizukami, M. Konczykowski, K. Matsuura, T. Watashige, S. Kasahara, Y. Matsuda, and T. Shibauchi, J. Phys. Soc. Jpn. **86**, 083706 (2017).

[16] S. Suzuki, K. Ohgushi, Y. Kiuchi, and Y. Ueda, Phys. Rev. B **82**, 184510 (2010).

[17] T. Goltz, V. Zinth, D. Johrendt, H. Rosner, G. Pascua, H. Luetkens, P. Materne, and H.-H. Klauss, Phys. Rev. B **89**, 144511 (2014).

[18] M. G. Vavilov and A. V. Chubukov, Phys. Rev. B **84**, 214521 (2011).

[19] R. M. Fernandes, M. G. Vavilov, and A. V. Chubukov, Phys. Rev. B **85**, 140512 (2012).

[20] Z.-C. Wang, C.-Y. He, S.-Q. Wu, Z.-T. Tang, Y. Liu, A. Ablimit, C.-M. Feng, and G.-H. Cao, J. Am. Chem. Soc. **138**, 7856 (2016).

[21] S. Matsuishi, Y. Inoue, T. Nomura, H. Yanagi, M. Hirano, and H. Hosono, J. Am. Chem. Soc. **130**, 14428 (2008).

[22] H. Chen, Y. Ren, Y. Qiu, W. Bao, R. H. Liu, G. Wu, T. Wu, Y. L. Xie, X. F. Wang, Q. Huang, and X. H. Chen, EPL Europhys. Lett. **85**, 17006 (2009).

[23] Z.-C. Wang, C.-Y. He, S.-Q. Wu, Z.-T. Tang, Y. Liu, and G.-H. Cao, Chem. Mater. **29**, 1805 (2017).

[24] Z.-C. Wang, C.-Y. He, Z.-T. Tang, S.-Q. Wu, and G.-H. Cao, Sci. China Mater. **60**, 83 (2017).

[25] S.-Q. Wu, Z.-C. Wang, C.-Y. He, Z.-T. Tang, Y. Liu, and G.-H. Cao, Phys. Rev. Materials **1**, 044804 (2017).

[26] See Supplemental Material at http://link.aps.org/supplemental/10.1103/PhysRevB.96.174522 for the XRD patterns of experimental and simulation data based on $I4/mmm$ and $P4/mmm$ space group. Bond length of Fe-As, bond angle of As-Fe-As and arsenic height from the Fe layer are summarized for all compositions. The magnetic susceptibility for the composition from $x = 0.00$ to 0.25 and the differential of the resistivity with respect to the temperature for all compositions are also represented.

[27] A. S. Sefat, A. Huq, M. A. McGuire, R. Jin, B. C. Sales, D. Mandrus, L. M. D. Cranswick, P. W. Stephens, and K. H. Stone, Phys. Rev. B **78**, 104505 (2008).

[28] N. Ni, M. E. Tillman, J.-Q. Yan, A. Kracher, S. T. Hannahs, S. L. Bud'ko, and P. C. Canfield, Phys. Rev. B **78**, 214515 (2008).

[29] C. M. Hurd, *The Hall Effect in Metals and Alloys* (Plenum Press, New York, 1972).

[30] Y. M. Dai, H. Miao, L. Y. Xing, X. C. Wang, P. S. Wang, H. Xiao, T. Qian, P. Richard, X. G. Qiu, W. Yu, C. Q. Jin, Z. Wang, P. D. Johnson, C. C. Homes, and H. Ding, Phys. Rev. X **5**, 031035 (2015).

[31] H. Miao, T. Qian, X. Shi, P. Richard, T. K. Kim, M. Hoesch, L. Y. Xing, X.-C. Wang, C.-Q. Jin, J.-P. Hu, and H. Ding, Nat. Commun. **6**, 6056 (2015).

[32] M. Abdel-Hafiez, S. Aswartham, S. Wurmehl, V. Grinenko, C. Hess, S.-L. Drechsler, S. Johnston, A. U. B. Wolter, B. Büchner, H. Rosner, and L. Boeri, Phys. Rev. B **85**, 134533 (2012).

[33] G. Tan, P. Zheng, X. Wang, Y. Chen, X. Zhang, J. Luo, T. Netherton, Y. Song, P. Dai, C. Zhang, and S. Li, Phys. Rev. B **87**, 144512 (2013).

[34] F. Hardy, P. Burger, T. Wolf, R. A. Fisher, P. Schweiss, P. Adelmann, R. Heid, R. Fromknecht, R. Eder, D. Ernst, H. v Löhneysen, and C. Meingast, EPL Europhys. Lett. **91**, 47008 (2010).

[35] A. Iyo, K. Kawashima, T. Kinjo, T. Nishio, S. Ishida, H. Fujihisa, Y. Gotoh, K. Kihou, H. Eisaki, and Y. Yoshida, J. Am. Chem. Soc. **138**, 3410 (2016).

[36] D. Mou, T. Kong, W. R. Meier, F. Lochner, L.-L. Wang, Q. Lin, Y. Wu, S. L. Bud'ko, I. Eremin, D. D. Johnson, P. C. Canfield, and A. Kaminski, Phys. Rev. Lett. **117**, 277001 (2016).

[37] J. Cui, Q.-P. Ding, W. R. Meier, A. E. Böhmer, T. Kong, V. Borisov, Y. Lee, S. L. Bud'ko, R. Valentí, P. C. Canfield, and Y. Furukawa, Phys. Rev. B **96**, 104512 (2017).

[38] K. Cho, A. Fente, S. Teknowijoyo, M. A. Tanatar, K. R. Joshi, N. M. Nusran, T. Kong, W. R. Meier, U. Kaluarachchi, I. Guillamón, H. Suderow, S. L. Bud'ko, P. C. Canfield, and R. Prozorov, Phys. Rev. B **95**, 100502 (2017).

[39] N. W. Salovich, H. Kim, A. K. Ghosh, R. W. Giannetta, W. Kwok, U. Welp, B. Shen, S. Zhu, H.-H. Wen, M. A. Tanatar, and R. Prozorov, Phys. Rev. B **87**, 180502 (2013).

[40] K. Hashimoto, T. Shibauchi, S. Kasahara, K. Ikada, S. Tonegawa, T. Kato, R. Okazaki, C. J. van der Beek, M. Konczykowski, H. Takeya, K. Hirata, T. Terashima, and Y. Matsuda, Phys. Rev. Lett. **102**, 207001 (2009).